LETTER • OPEN ACCESS

The rapid rise of severe marine heat wave systems

ENVIRONMENTAL RESEARCH
CLIMATE

LETTER

The rapid rise of severe marine heat wave systems

J Xavier Prochaska*, Claudie Beaulieu and Katerina Giamalaki

Ocean Sciences, University of California, Santa Cruz, 1156 High St, Santa Cruz, CA 95064, United States of America
* Author to whom any correspondence should be addressed.

E-mail: jxp@ucsc.edu

Keywords: marine heat wave, sea surface temperature, ocean heating

OPEN ACCESS

RECEIVED
2 September 2022

REVISED
27 January 2023

ACCEPTED FOR PUBLICATION
14 April 2023

PUBLISHED
2 May 2023

Abstract

We introduce a new methodology to study marine heat waves (MHWs), extreme events in the sea surface temperature (SST) of the global ocean. Motivated by previously large and impactful MHWs and by theoretical expectation that the dominant heating processes coherently affect large regions of the ocean, we introduce a methodology from computer vision to construct marine heat wave systems (MWHSs) – the collation of SST extrema in dimensions of area and time. We identify 649 475 MHWSs in the 37 year period (1983–2019) of daily SST records and find that the duration $t_{\rm dur}$ (days), maximum area $A_{\rm max}$ (km^2), and total 'volume' $V_{\rm MHWS}$ (days km^2) for the majority of MHWSs are well-described by power-law distributions: $t_{\rm dur}^{-3}$, $A_{\rm max}^{-2}$ and $V_{\rm MHWS}^{-2}$. These characteristics confirm SST extrema exhibit strong spatial coherence that define the formation and evolution of MHWs. Furthermore, the most severe MHWSs deviate from these power-laws and are the dominant manifestation of MHWs: extrema in ocean heating are driven by the ∼200 systems with largest area and duration. We further demonstrate that the previously purported rise in the incidence of MHW events over the past decade is only significant in these severe systems. A change point analysis reveals a rapid increase in days under a severe MHW in most regions of the global ocean over the period of 2000–2005. Understanding the origin and impacts of MHWs in the current and future ocean, therefore, should focus on the production and evolution of the largest-scale and longest-duration heating phenomena.

1. Introduction

With the incontrovertible warming of the Earth's ocean, both at the surface and at depth (e.g. Roemmich *et al* 2015, Bulgin *et al* 2020, Johnson and Lyman 2020), extreme heating events are increasing both in frequency and intensity (see Oliver *et al* 2021, for a review). Termed marine heat waves (MHWs), analogs to the atmospheric extrema that occur over land (e.g. Perkins-Kirkpatrick 2015), these events represent periods of elevated and sustained ocean warming relative to the recorded climatology. As climate change continues to increase the temperature of our ocean's surface, MHWs are likely to become more frequent and impactful on our ecosystem.

Besides serving as putative signatures of global warming, MHWs have potentially negative impacts on ocean life, especially when they come in close contact with coastal areas (e.g. Smith *et al* 2023). Reported consequences on marine life include harmful algal blooms (McCabe *et al* 2016), shifts in species range (e.g. Cavole *et al* 2016, Lenanton *et al* 2017), and even local extinctions (Straub *et al* 2022). The influence of MHWs have also been experienced in the economic sector, with instances of MHWs affecting aquaculture or important fisheries (e.g. Mills *et al* 2013, Barbeaux *et al* 2020). The largest MHW ever recorded, dubbed the 'Warm Blob', occurred in the Northeast Pacific Ocean between 2013 and 2015. Regions of the blob exhibited maximum sea surface temperature (SST) that reached 6 °C above average, sufficient to greatly impact the western seaboard (e.g. Bond *et al* 2015).

The primary observable for quantifying MHWs is the SST, recorded across the global ocean by remote sensing satellites supplemented by *in-situ* observations (e.g. Reynolds *et al* 2007). With such datasets now spanning nearly 40 years, one may construct a baseline of SST measurements and search for excursions

representing extrema. To date, the majority of MHW literature have defined these phenomena on small scales, typically the $0.25° \times 0.25°$ discretization of the Level 4 datasets provided for SST. The oft-used methodology of Hobday *et al* (2016), for example, defines a marine heat wave event (MHWE) as any 0.25° cell with SST exceeding the 90th percentile climatology for at least 5 consecutive days. This and subsequent analyses have explored the incidence of such MWHEs across time and by region and their potential drivers (e.g. Frolicher *et al* 2018, Oliver *et al* 2018, Holbrook *et al* 2019, Jacox *et al* 2020, Laufkötter *et al* 2020, Sen Gupta *et al* 2020, Vogt *et al* 2022) and recent work has constructed predictive models based on numerical models and machine-learning approaches (e.g. Giamalaki *et al* 2022, Jacox *et al* 2022).

While the physical mechanisms that generate MHWEs have not yet been firmly established (Oliver *et al* 2021), the leading forcings are radiative heating and wind. The latter impacts surface cooling, ocean currents (i.e. advection), and the depth of the mixed layer which in turn modulates SST. These forcings generally act on large spatial scales (>100 km) and often for relatively long durations ($\gg$5 days). Indeed, the community has identified several long-term and large heating events (e.g. the Warm Blob) that have had significant impacts on the environment and marine life throughout an entire ocean basin (Cavole *et al* 2016, Zhu *et al* 2017, Piatt *et al* 2020, Rogers *et al* 2021). Therefore, we consider MHW phenomena on larger scales than most of the previous works.

In this paper, we develop a new methodology to characterize SST extrema with the primary goal to account for spatial and temporal coherence in MHWs. Specifically, we introduce marine heat wave systems (MHWSs) that are the agglomeration of MHWEs coincident in area and time. Our analysis examines the distributions of sizes and durations and 'volume' of these collated systems. We then show that the largest systems, in space and time, dominate ocean extremes and exhibit the greatest increase of occurrence in the warming ocean.

2. Data and methods

2.1. Dataset

As with several previous treatments of MHWs, our analysis starts from the National Oceanic and Atmospheric Administration optimal interpolation SST (NOAA OI SST) dataset (Reynolds *et al* 2007), a global grid with 0.25° angular resolution and daily outputs spanning nearly four decades (1982–2019). While there exists a wide range of SST datasets available for exploring extrema on the ocean surface, this product has several positive characteristics for such analyses: (i) daily cadence; (ii) coverage of the full ocean; (iii) synthesis of satellite and *in-situ* sensors to compensate for clouds and compromised measurements; (iv) relatively high spatial-resolution (0.25°); and (v) nearly 40 years of continuous coverage. Together these enable the assessment of MHW phenomena from spatial scales of $\sim$10 km to entire basins, and on timescales of $\sim$1 week to multiple years. At the same time, one should be cautious that the assimilation and interpolation schema of NOAA OI may introduce correlations on time-scales of several days or on spatial scales set by, e.g. cloud complexes. These effects, however, are unlikely to significantly impact the large-scale and longer-duration phenomena examined in this study.

2.2. MHWE

We follow the definition of MHWE from Hobday *et al* (2016). This definition is based on the SST climatology, which refers to the distribution of SST at a given location on a given day of the year (DOY). As we are interested in extrema, we measure percentiles of the SST distribution to establish a threshold T_{thresh} which defines an extreme SST excursion. We adopt the 90th percentile T_{90}, i.e. $T_{\text{thresh}} = T_{90}$. Given T_{90} derived from the climatology, one defines a MHWE for a given cell as any interval where the SST exceeds T_{90} for 5 or more consecutive days. Furthermore, sets of MHWEs that occur within 2 days of one another (e.g. a gap of 1 day between a pair of MHWEs) are collated into a single MHWE. By construction, every position on the ocean will have SST values that exceed T_{90} for $\sim$10% of the climatological interval and therefore MHWEs may be expected to span the entire ocean. This definition follows Hobday *et al* (2016), differing only in the period used to define the climatology where we have adopted the full analysis period instead of the first 20 years (see supplementary section).

2.3. MHWS

The basic definition of a MHWS is straightforward: a MHWS is the collection of all MHWEs that connect in space and time. A trivial example is two neighboring MHWEs with identical start and end times, e.g. at identical latitude but offset by 0.25° in longitude. These two MHWEs comprise a single MHWS with twice the area of each MHWE and with identical duration. Or, if the heating event is dynamic, the MHWS may manifest first in one location of the ocean and 'migrate' by connecting neighboring MHWEs that overlap

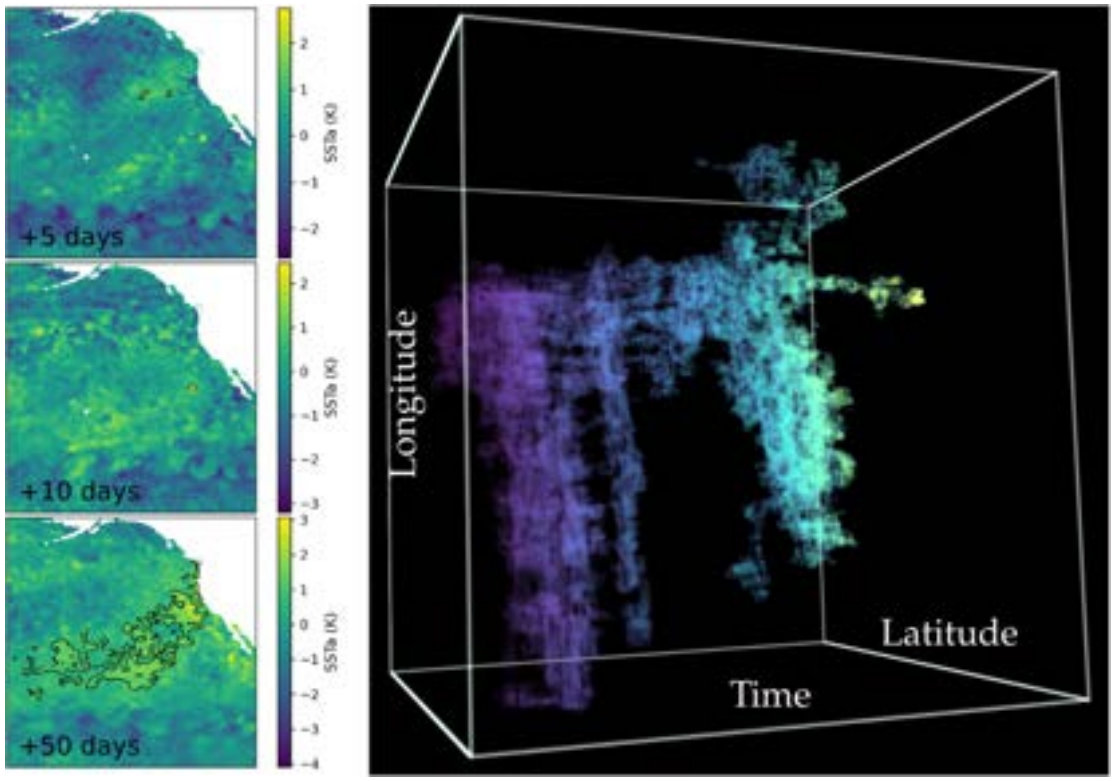

Figure 1. Example of a MHWS. The left panels show anomalous SST maps for a 70° × 70° region in the Pacific centered on $lat, lon \approx 26°, 217°$ on the dates of 31 October 1995, 5 November 1995, and 15 December 1995 (top to bottom). In each panel, the black contours define the regions that satisfy the MHWE definition and contribute to the MHWS, i.e. all have adjacent cells in location or time. The right-hand panel is a 3D-rendering of the MHWS where the color-coding indicates time (purple to yellow). This MHWS had a duration of $t_{dur} \approx 307$ *days*, a maximum area $A_{max} \approx 6500000$ km^2, and a $V_{MHWS} \approx 515000000$ days km^2.

in time. Most complex is the connection of multiple well-separated and long-lived events by an intermediate (in time and space) warming period.

Figure 1 illustrates one MHWS example from the Pacific Ocean centered at $lat, lon \approx 26°, 217°$ and with start,end times: $t_s, t_e =$ 26 October 1995, 27 August 1996. The left panels show anomalous SST (SSTa) maps around the region on several days between t_s, t_e and highlight cells where the SST values exceed T_{90}. The right-hand panel shows a rendering of the MHWS in its three dimensions of space and time. We define one 'cube' in this 3D framework as a voxel; it has units of km^2 days. This MHWS example, comprised of 44 065 individual MHWEs, has a total 'volume' of 516 746 800 km^2 days. One physical motivation for introducing MHWS's is highlighted by figure 1: by December 2015 the MHWS extends many tens of degrees on the ocean surface and eventually reaches a maximum area on a single day of $A_{max} = 6500934$ km^2, indicating a wide-spread forcing mechanism. Furthermore, the total duration ($t_{dur} = 307$ days) is much longer than the maximum of its constituent MHWEs (133 days). To understand the origin and impacts of MHWs, it is essential to examine their total duration and spatial extent.

While statistics on the number and duration of individual MHWEs in this region might indicate a significant warming on their own, the construction of a MHWS explicitly captures the correlations in space and time of the extrema. Furthermore, the MHWS definition captures the translation of extrema across the ocean surface owing to ocean dynamics or evolving heating processes. In practice, the MHWS is the set of connected voxels in the 3D space-time satisfying the MHWE definition. Every pair of neighboring voxels, in date or location, is grouped together and the contiguous set of all voxels defines one MHWS.

The algorithm implemented to construct the MHWSs was taken from Shapiro and Stockman (2001) who introduced it for computer vision tasks. We drew inspiration from an application in astronomy where the authors map Hydrogen emission across the sky and in velocity (Cantalupo *et al* 2014). We also note the treatment is similar to the methodology of Laufkötter *et al* (2020) for MHWs. The only significant deviations in our algorithm from that of Shapiro and Stockman (2001) were modifications for our spherical geometry and a restriction that prevents MHWSs from spanning across multiple basins.

The primary adjustable parameter for the algorithm is the minimum number of adjacent voxels required to define a collection. In our implementation, we have adopted the minimum, i.e. a single neighboring pair in space or time. Experimenting with larger values, we find the primary effect is to eliminate many of the

Table 1. Definition of basins adopted.

Basin	Boundary	Location	Range
Indian	E/W	145E	90S, 0N
Indian	E/W	100E	0N, 31N
Indian	E/W	20E	90S, 0N
Indian	S/N	0N	145E, 100E
Pacific	E/W	70W	90S, 0N
Pacific	S/N	66N	100E, 120W

The Boundary separates the basins from East to West (E/W) or South to North (S/N) at the longitude/latitude Location given. The Range of the Boundary is provided by the final column.

minor MHWS. Increasing this minimum will also split apart a number of the MHWS with large V_{MHWS} into multiple, but still large volume MHWS. Qualitatively, there is little effect on the results or characteristics of the MWHS population unless one adopts a value much larger than 1.

When defining MHWSs, we have chosen to restrict the spatial collation of MHWEs by major ocean basin such that a given MHWS is not allowed to span across more than one basin. While there may be physical influences that link extrema in one basin to another, our experiments identified linkages that may be non-physical and we chose to suppress this behavior. This included one example that traversed the entire globe with a duration of many years. To enforce the basin separation, we created boundaries with a set of lines of constant latitude or longitude (table 1). In practice, this primarily affects MHWSs that would have spanned across the eastern Pacific islands and several that would connect the Indian Ocean to the Atlantic around Cape Agulhas.

We then calculate a set of simple metrics that characterize a MHWS. Each voxel has a date t_i and a measured area A_i given its location. The total duration t_{dur} is the time interval in days between the earliest time $t_s = min(t_i)$ and latest time $t_e = max(t_i)$ for the voxels defining the MHWS,

$$t_{\mathrm{dur}} = t_e - t_s + 1. \tag{1}$$

The maximum area A_{max} is largest area calculated for the MHWS on a single day during its duration, measured in km^2.

$$A_{\mathrm{max}} = max(A_{\mathrm{day}}) \tag{2}$$

where

$$A_{\mathrm{day}}(t) = \sum_i A_i\,(t_i = t). \tag{3}$$

The MHWS volume V_{MHWS} is the simple sum of the volume of each voxel $V_i = A_i\,t_i$ with unit km^2 days,

$$V_{\mathrm{MHWS}} = \sum_i V_i\,. \tag{4}$$

We also consider a characteristic area $\bar{A}$ defined as

$$\bar{A} \equiv \frac{V_{\mathrm{MHWS}}}{t_{\mathrm{dur}}}, \tag{5}$$

which describes the average area occupied by an MHWS during its duration, measured in km^2.

Table 2 lists all of the MHWSs for the fiducial climatology and their salient properties.

2.4. Analysis of MHWS time series

To characterize and quantify changes in MHWS over 1983–2019, We perform trend detection and a change point analysis. A Mann–Kendall (MK) trend test (Mann 1945, Kendall 1948), which is a nonparametric approach, is used to detect trends. For a given time series $X_t, t = 1, 2 \ldots, n$, the null hypothesis assumes it is independently distributed, and the alternative hypothesis is that there exists a monotonic trend. The MK statistic is given by

$$S = \sum_{k=1}^{n-1} \sum_{j=k+1}^{n} sign(X_j - X_k) \tag{6}$$

Table 2. Marine heat wave systems.

ID	Lat (deg)	Lon (deg)	Start	t_{dur} (days)	A_{max} (km^2)	V_{MHWS} (days km^2)
1	−78.375	166.000	5 January 1983	5	311	1.56×10^3
2	−77.207	168.606	26 March 1983	52	3.86×10^4	9.42×10^5
4	−78.292	166.347	22 July 1983	8	1.26×10^3	8.47×10^3
5	−65.114	189.869	17 March 1983	366	2.74×10^6	1.81×10^8
6	−77.463	167.973	4 September 1983	17	1.24×10^4	1×10^5
7	−78.327	166.968	20 September 1983	17	2.19×10^3	2.83×10^4
9	−71.685	175.861	3 March 1984	293	8.42×10^5	7.03×10^7
11	−78.375	166.586	6 January 1985	6	1.09×10^3	5.92×10^3
12	−78.138	166.940	17 July 1985	31	4.5×10^3	8.64×10^4
13	−78.142	166.616	23 August 1985	20	3.18×10^3	4.97×10^4
14	−77.999	166.855	15 September 1985	46	5.68×10^3	1.02×10^5
16	−61.980	194.638	28 March 1985	1091	5.69×10^6	1.39×10^9
19	−78.274	166.658	6 October 1986	35	1.73×10^3	3.75×10^4
20	−78.375	165.875	23 February 1987	5	156	779
22	−77.614	166.100	9 August 1987	11	1.14×10^4	8.79×10^4
24	−77.713	165.316	6 December 1987	33	8.69×10^3	1.77×10^5
25	−75.173	173.036	5 December 1987	94	1.12×10^5	4.03×10^6
26	−65.714	248.850	19 March 1988	455	5.5×10^6	6.54×10^8
27	−77.153	166.967	15 September 1988	58	4.68×10^4	9.36×10^5
29	−78.375	166.234	6 March 1989	6	623	3.58×10^3
30	−76.640	169.068	19 March 1989	33	9.11×10^4	1.6×10^6
31	−75.726	174.695	23 August 1989	203	3.08×10^5	1.35×10^7
32	−78.375	166.135	18 March 1990	9	467	4.05×10^3
33	−71.235	197.930	22 January 1990	323	1.3×10^6	9.98×10^7
34	−75.777	182.065	20 November 1990	110	2.94×10^5	9.74×10^6
35	−45.827	223.795	31 December 1990	1211	2.09×10^7	5.95×10^9

where X_t represents the number of days in a MHW at time $t(t = 1, \ldots, n)$, X_j and X_k represent the later-observed and earlier-observed values, respectively $(j > k)$ and

$$sign(x) = \begin{cases} 1, x > 0, \\ 0, x = 0, \\ -1, x < 0. \end{cases} . \tag{7}$$

The statistic S is standardized such that:

$$Z = \begin{cases} \frac{(S-1)}{\sqrt{V(S)}}, S > 0, \\ 0, S = 0, \\ \frac{(S+1)}{\sqrt{V(S)}}, S < 0, \end{cases} \tag{8}$$

where the variance of S is given by $V(S) = [n(n-1)(2n+5) - \sum_{j=1}^{p} t_j(t_j-1)(2t_j+5)]/18$ and t_j is the number of data in the tied group and p is the number of groups of tied ranks. The statistic Z follows a standard Normal distribution with E(Z) = 0 and V(Z) = 1.

An estimate of the trend is given by the Sen's slope. A set of slopes for all pairs of data that were used to compute S is computed first:

$$d_k = \frac{(X_j - X_i)}{j - i} \tag{9}$$

for $(1 <= i < j <= n)$, where d_k is the slope between data points X_j and X_i. The Sen's slope b is then calculated as the median from all slopes: $b = median(d_k)$.

To complement a trend analysis and quantify the timing of the rapid increase in severe MHW days, we perform a change point analysis using the non-parametric Pettitt test (Pettitt 1979) due to the non-Gaussian nature of extreme events. Here the null hypothesis is that the time series follow one or more distributions that have the same location parameter (no change), against the alternative that a change point exists. The non-parametric statistic is defined as:

$$K_T = max|U_{t,T}|, \tag{10}$$

where

$$U_{t,T} = \sum_{i=1}^{t} \sum_{j=t+1}^{T} sign(X_i - X_j). \tag{11}$$

The most likely timing for a change-point is K_T and its significance is approximated by

$$p \approx 2 \exp \frac{-6K_T^2}{T^3 + T^2}. \tag{12}$$

Both the Pettitt test and MK trend test are applied using the `R` package `trend` (Pohlert 2020).

3. Results

We have identified and characterized MHWSs within the 1983–2019 period. Restricting each MHWS to reside with a single basin, we recover 649 475 unique MHWSs from 49 034 524 MHWEs. The nearly 100× reduction in the number of phenomena demonstrates the strong spatial correlation in MHWs. The following subsections present the primary measurements and results on the MHWSs.

3.1. MHWS properties

Figure 2 presents histograms of the duration t_{dur}, maximum area A_{max}, and total volume V_{MHWS} for the full distribution of 649 475 MHWSs from 1983–2019 (inclusive). The t_{dur} distribution (figure 2(a)) peaks at the minimum value which defines a MHWE (5 days) and declines systematically to the maximum value (≈4000 days). We have fit the t_{dur} distribution with a simple power-law $\Phi(t_{\text{dur}}) = C t_{\text{dur}}^{-\alpha}$ using standard maximum likelihood techniques for a discrete valued distribution. Remarkably, the entire distribution—spanning three orders-of-magnitude in t_{dur}—is very well described by a single power-law with exponent $\alpha_t = -3.0$. This 'scale-free' distribution is very steep, i.e. MHWSs are overwhelmingly dominated in number by short-term events. We find approximately 90% of the MHWSs last fewer than 15 days. Despite this, we demonstrate below that these short-duration MHWSs contribute negligibly to the integrated extrema on the ocean's surface. It is instead the tail of the t_{dur} distribution that dominates.

Turning to A_{max} (figure 2(b)), one end of the distribution shows a small number of MHWS with small area. These are systems in the polar regions where $[0.25°]^2$ corresponds to a small area (≈100 km^2); they are relatively rare and largely inconsequential. The total distribution peaks at $A_{\text{max}} \approx 10^3$ km^2 and then follows a power-law $\Phi(A_{\text{max}}) \propto A_{\text{max}}^{-2.1}$ across four orders of magnitude. With an exponent of ≈ -2, markedly shallower than the t_{dur} distribution, this implies that each logarithmic interval of MHWS in A_{max} covers the same integrated area. Stated another way, the spatial coherence of SST extrema yields a sufficient number of large-area MHWS to have high impact as extrema on the ocean's surface.

The very largest MHWSs exhibit $A_{\text{max}} > 10^6$ km^2 and there are tens of MHWSs during the period with $A_{\text{max}} > 10^7$ km^2 (i.e. $> 10^3$ km in radius) or roughly 20% of the Pacific ocean. Evidently, the mechanisms driving MHWs are capable of generating basin-scale extrema.

Lastly, we examine the values of V_{MHWS} for the MHWSs which describe the combined duration and sizes of the systems. The V_{MHWS} distribution (figure 2(c)) shows similar characteristics as A_{max}: there is a small set of systems with very low V_{MHWS} ($<10^4$ vox) followed by the primary set which tracks a steep power-law profile. Analyzing the MHWSs with $V_{\text{MHWS}} > 10^5$ vox yields the power-law $\Phi(V_{\text{MHWS}}) \propto V_{\text{MHWS}}^{-1.9}$ which describes the data well until $V_{\text{MHWS}} \approx 10^8$ vox. As with A_{max}, this indicates that the majority of MHWSs occupy the same integrated volume per logarithmic bin. Spatial coherence in SST extrema generates very high V_{MHWS} MHWS that contribute significantly to MHWs. Furthermore, beyond $\approx 10^8$ vox there is yet another flattening in the distribution which has even greater implications for MHWs.

The importance of this flattening in $\Phi(V_{\text{MHWS}})$ is most apparent when one considers the total volume of MHWSs during the entire period. Figure 2(d) presents the cumulative contribution of MHWSs to the total as a function of V_{MHWS}. The systems with lower values ($V_{\text{MHWS}} < 10^5$ vox) dominate in number but contribute $< 5\%$ of the total vox of the ocean in a MHW state. We refer to these as 'minor' MHWSs and interpret them as non-impactful fluctuations just above the 90th percentile in SST. At $V_{\text{MHWS}} \approx 10^5$ vox, the distribution transitions to the $\alpha \approx -2$ power-law implying the total volume per logarithmic bin is independent of V_{MHWS}, i.e. there is a linear increase in the total vox with each logarithmic interval in V_{MHWS} (figure 2(d)). We define these as the 'moderate' set of MHWSs.

Last, and most striking, for MHWSs with $V_{\text{MHWS}} > 10^8$ vox, the total vox per logarithmic bin *increases*. In fact, these 226 'severe' MHWSs comprise ≈70% of the total ocean designated as satisfying a MHW condition. Therefore, the contribution of these severe MHWSs to MHW extrema exceeds the combined

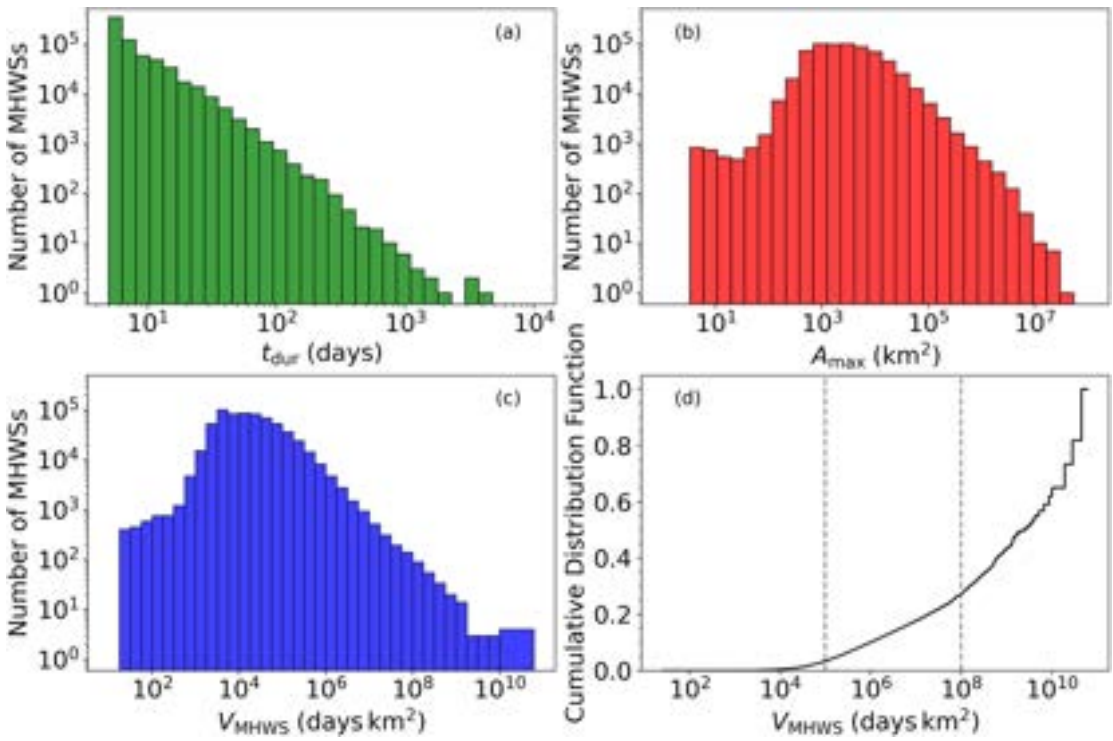

Figure 2. Histograms of the primary characteristics of the MHWS: duration t_{dur} (a), maximum area A_{max} (b), and volume V_{MHWS} (c). The t_{dur} distribution is well-described by a power-law with exponent $\alpha \approx -3$. The A_{max} and V_{MHWS} distributions each show a small set of systems with low values; these arise primarily in the Arctic and Antarctic Oceans and have negligible contribution. The remainder of these distributions are each well-fit by a single power-law with exponents $\alpha \approx -2$. At the very highest of A_{max} and V_{MHWS}, however, there is a flattening and these severe MHWSs dominate the cumulative sum of each distribution. This is illustrated in (d) which shows the cumulative distribution function of V_{MHWS}. The dashed lines delineate three classifications of MHWSs: (i) minor, $V_{MHWS} < 10^5$ vox; (ii) moderate, $10^5 \leqslant V_{MHWS} < 10^8$ vox; and (iii) severe, $V_{MHWS} \geqslant 10^8$ vox. One notes the negligible contribution of the minor MHWS, the roughly linear contribution of the moderate MHWS in logarithmic steps of V_{MHWS}, and the great contribution of the severe MHWS.

effect of all smaller systems. These 'severe' MHWSs lie in stark contrast to the main population and, as demonstrated below, are the dominant phenomena driving the rise in ocean surface heating.

The single largest MHWS, which includes the infamous Pacific blob, has persisted in the Pacific Ocean since the end of 2009. We provide an animation of this MHWS (and other severe examples) which shows it is the agglomeration of many large structures throughout the full basin. We expect that these were generated by several, distinct forcing mechanisms and one might be inclined to modify the MHWS definition to break this MHWS into smaller ones. We emphasize, however, that most of these would also satisfy the severe definition and the principle conclusions of this work would still hold.

For the remainder of the paper we adopt the following categories for MHWSs based on the statistics above: (i) minor, $V_{MHWS} < 10^5$ vox (which corresponds to 85.37% of all MHWS); (ii) moderate, $10^5 \leqslant V_{MHWS} < 10^8$ vox (14.6% of all MHWS); and (iii) severe, $V_{MHWS} \geqslant 10^8$ vox (0.03% of all MHWS).

3.2. Geographic distribution of MHWSs

The spatial distribution of MHWS may provide insight into the forcing mechanisms that generate them and also highlights portions of the ocean (and coastlines) most impacted by them. Figure 3(a) shows the geographic, cumulative distribution of the minor MHWSs defined as the number of days during 1983–2019 that a given location exhibited a minor MHWS. As might be expected, these are roughly uniformly distributed across the ocean with each location exhibiting an average of ≈40 extrema days over the full period. The only areas with an excess of these minor MHWSs are the most dynamic regions of the ocean, e.g. the Gulf stream and the Antarctic Circumpolar Current (ANT). We infer that the complex currents of these regions lend to larger fluctuations in SST and therefore shorter duration MHWSs (i.e. fewer moderate and severe systems; see also Oliver *et al* 2021). In contrast, the highest latitudes exhibit a modest deficit of the minor MHWSs (especially the Arctic Ocean). We believe this is due to the greater spatial coherence in SST which lends to a higher incidence of large-area moderate and severe MHWSs.

A similar map for the moderate MHWSs (figure 3(b)) shows greater geographical variation. There is an elevated incidence in these MHWSs near several coastlines, e.g. the Gulf of Mexico, Bay of Bengal, Hudson

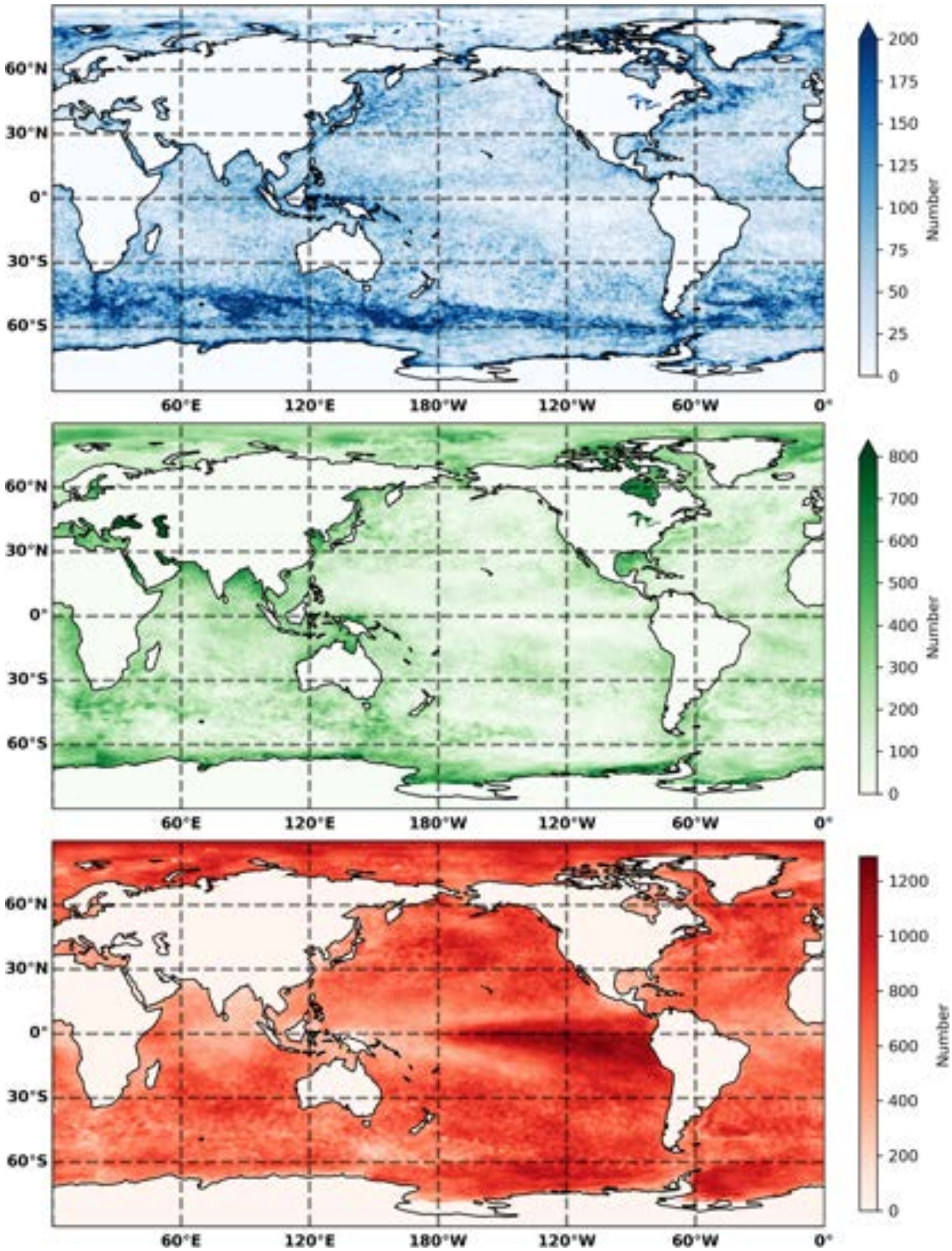

Figure 3. The panels show the number of days that each location spent in a MHWS during the full period (1983–2019) in one of the three categories: (a) minor, (b) moderate, (c) severe. Each category shows a progressively higher number of days and greater structure in the spatial distribution. We identify the highest incidence of minor MHWSs within the most dynamic regions of the ocean (e.g. the Gulf Stream, the ANT). In contrast, the moderate MHWSs occur primarily in coastal regions (e.g. Bay of Bengal, Gulf of Mexico). Last, the severe MHWSs tend to basin-wide regions and especially the Equatorial Pacific.

Bay, waters off western Africa, and the north coast of Australia. In contrast, the Pacific Ocean and Northern Atlantic show fewer moderate MHWSs. Overall, these moderate MHWSs track extrema in modest sized areas with significant coastlines while generally avoiding the major basins. Therefore, they may be more impactful on human activity than regions of the open ocean.

Last, figure 3(c) reveals the regions most frequently affected by severe MHWSs. These are the Arctic Ocean (which contains over 20 distinct severe MHWSs), the Indian Ocean, the Pacific Ocean, and the Antarctic Ocean. The high incidence of severe MHWSs in the Arctic Ocean reflects recent warming in that

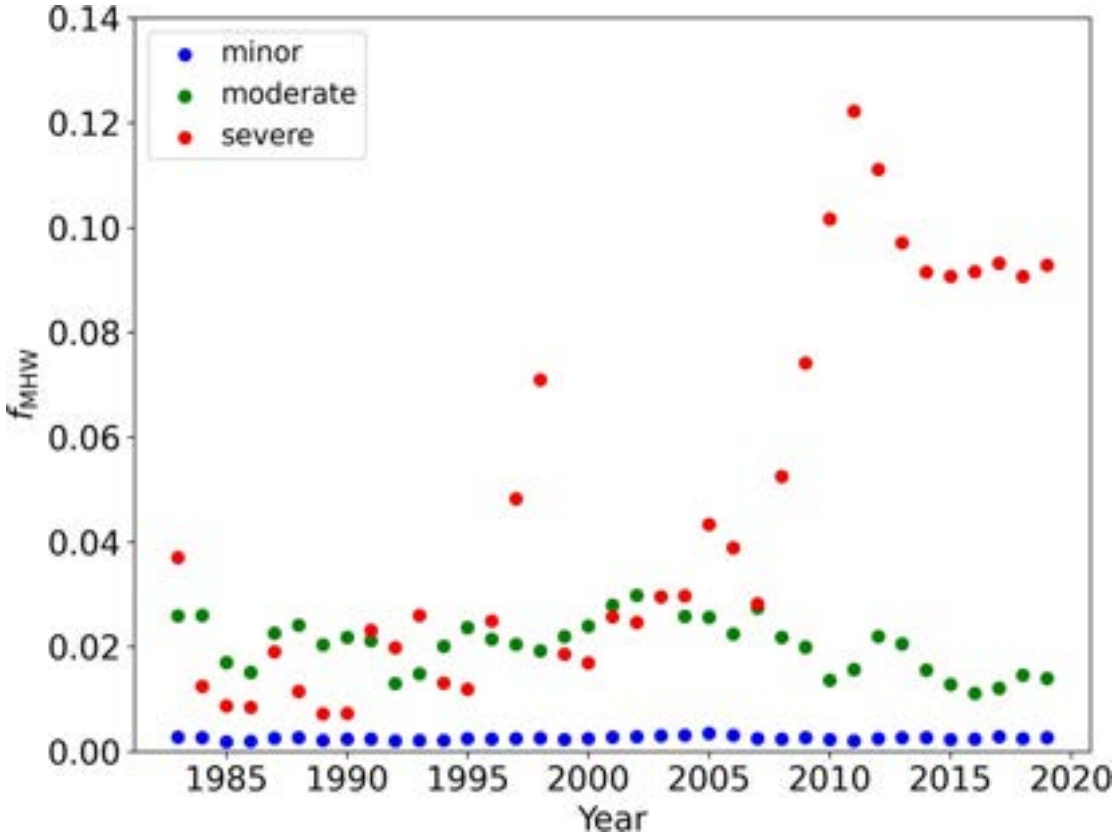

Figure 4. Time series for the fraction of the ocean surface f_{MHW} that in a given year exhibits one of the three MHWS states: minor (blue), moderate (green), severe (red). The minor MHWSs affect a very small fraction of the ocean surface ($\ll 1\%$) with little variation in time. In contrast, the severe events affect $\approx 10\%$ and show an $\approx 5\times$ increase over the past ≈ 15 years.

basin but also the relative coherence of SST at high latitudes. The excess of severe MHWSs in the Indian and Pacific oceans indicate the MHW events in those regions are especially coherent and extended in duration. The regions that are avoided by severe MHWSs are also noteworthy, e.g. the ACC, Bay of Bengal, Gulf of Mexico. We suggest the extrema in these areas are dominated by local effects and remain relatively isolated from the large-scale circulation and heating of the main basins.

3.3. Time evolution

In figure 4, we explore time evolution in the global incidence of MHWSs separated by the minor, moderate, and severe categories. Specifically, we plot the fraction of the ocean surface in a MHWS each year defined as $f_{MHW} = V_{MHWS}/(A_{ocean} \times 365 \text{ days})$ with A_{ocean} the total area of the ocean in (691 150 cells of $[0.25°]^2$ or $\approx 364\,000\,000$ km^2). We find the minor MHWS cover less than 1% of the ocean per year and show small variations ($\approx 20\%$) between years. Similarly, the moderate MHWS have $f_{MHW} \approx 2\%$ and also have relatively small temporal change across the period, aside from an approximately 30% decline in the last 10 years. The most significant trend is the remarkable rise of severe events after ≈ 2010, an $\approx 100\% - 300\%$ increase in f_{MHW} to cover more than 5% of the ocean surface each year. Over the past ≈ 10 years, the ocean has exhibited an $\approx 2\times$ increase in extrema, with essentially all of this attributed to severe MHWSs that cover large regions of the ocean for very long times.

We now quantify changes in MHWS over 1983–2019 and examine the presence of rapid increase in severe MHWS within sub-regions of the ocean. We perform trend detection and a change point analysis to characterize changes. The results presented in figure 4 imply a significant rise in MHWs manifest in the severe MHWS beginning approximately 15 years ago.

Results are presented in table 4. This analysis reveals a significant ($p < 0.05$) monotonic increase in severe MHW days in 10/11 regions, with the exception of the Antarctic Circumpolar Current (ANT) region that exhibits a significant decrease in severe MHW days over the time period.

To complement a trend analysis and quantify the timing of the rapid increase in severe MHW days, we apply the Pettitt test to the total sample (global) and 11 distinct regions (figure 5). Specifically, we examined the annual time series of the number of voxels in a MHWS restricted to these various geographical regions (defined by table 3).

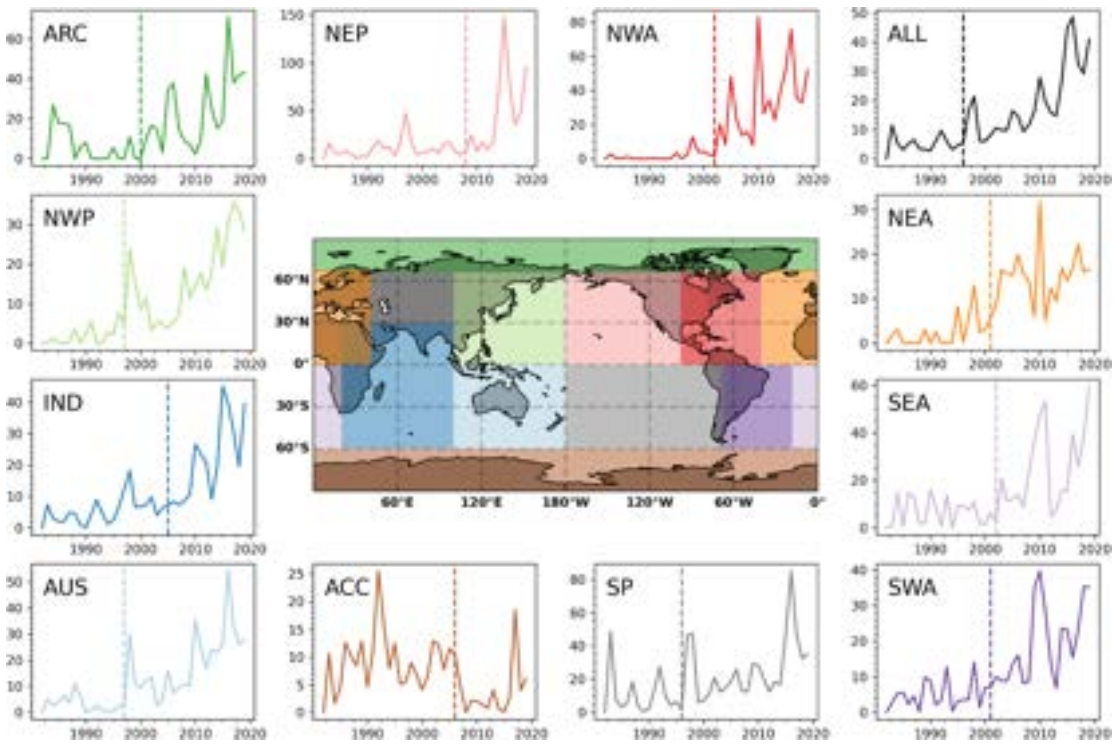

Figure 5. Number of days that each region spent in a severe MHWS during the full period. The map shows the breakdown of regions and their corresponding time series are plotted in the same color. The regions analyzed are (see table 3): Arctic (ARC), Northwest Pacific (NWP), Indian Ocean (IND), Australian seas (AUS), Northeast Pacific (NEP), Antarctic (ANT), Northwest Atlantic (NWA), South Pacific (SP), Northeast Atlantic (NEA), Southeast Atlantic (SEA), Southwest Atlantic (SWA) and global (ALL). Vertical dashed lines indicate where a changepoint has been detected (Pettitt test, 5% critical level). In all regions a changepoint is detected and corresponds to a rapid increase in severe MHWS days, except for the Southern Ocean showing a decrease.

Table 3. Regions for analysis.

Region	Latitudes	Longitudes
NWP	0N–66N	100E–179W
AUS	59S–0N	100E–179W
IND	59S–30N	20E–100E
ARC	66N–89N	0E–0W
NEA	0N–68N	39W–41E
NEP	0N–66N	179W–77W
NWA	0N–66N	97W–39W
SEA	59S–0N	17W–20E
SWA	59S–0N	69W–17W
SP	59S–0N	179W–66W
ACC	89S–59S	0E–0W

The latitude and longitude ranges define the 11 regions considered in the change point analysis. Acronyms are: Arctic (ARC), Northwest Pacific (NWP), Indian Ocean (IND), Australian seas (AUS), Northeast Pacific (NEP), Antarctic (ANT), Northwest Atlantic (NWA), South Pacific (SP), Northeast Atlantic (NEA), Southeast Atlantic (SEA), Southwest Atlantic (SWA). For the NEP and NWA regions, we included custom masks to exclude the Gulf of Alaska and Pacific waters, respectively.

Table 4 lists the results of this analysis. We find each region exhibited a statistically significant ($p < 0.05$) change-point during the full period. The majority of the change points occur during the years 2000–2005, consistent with our inferences from figure 4. Specifically, an increase in severe MHW days is detected at that

Table 4. Change point analysis.

Region	Slope	p-value	Changepoint	p-value
		Severe		
ACC	−0.24	0.0068	2006.0	0.0032
ALL	0.67	4.2×10^{-8}	1996.0	0.00 011
ARC	0.64	0.00 085	2000.0	0.004
AUS	0.74	2.3×10^{-6}	1997.0	9.4×10^{-5}
IND	0.57	1×10^{-7}	2005.0	0.00 018
NEA	0.52	1.2×10^{-7}	2001.0	1.1×10^{-5}
NEP	0.66	0.00 021	2008.0	0.0092
NWA	1.13	1.4×10^{-8}	2002.0	4.4×10^{-6}
NWP	0.71	3×10^{-9}	1997.0	5.4×10^{-5}
SEA	0.63	0.00 036	2002.0	0.0013
SP	0.71	0.00 039	1996.0	0.015
SWA	0.61	1.6×10^{-6}	2001.0	0.00 011
		Moderate		
ACC	−0.12	9.4×10^{-7}	2006.0	3.5×10^{-5}
ARC	−0.21	0.00 078	2010.0	0.026
AUS	−0.02	0.61	2009.0	0.63
IND	−0.01	0.59	2009.0	0.72
NEA	0.06	0.0018	1995.0	0.015
NEP	−0.06	0.0092	2007.0	0.066
NWA	0.07	0.12	1993.0	0.0061
NWP	−0.00	0.84	2010.0	0.16
SEA	−0.12	0.0086	2003.0	0.037
SP	−0.06	0.0086	2005.0	0.028
SWA	−0.07	0.0042	2006.0	0.00 082
		Minor		
ACC	−0.01	6.3×10^{-7}	2006.0	6.2×10^{-5}
ARC	0.00	0.069	1999.0	0.026
AUS	0.00	0.95	1998.0	0.2
IND	0.00	0.5	2000.0	0.34
NEA	0.01	0.0001	1996.0	8.2×10^{-5}
NEP	0.00	0.74	2013.0	0.66
NWA	0.01	0.003	1997.0	0.00 021
NWP	0.00	0.0035	1998.0	0.0012
SEA	−0.00	0.2	1991.0	0.04
SP	0.00	0.89	2007.0	0.89
SWA	−0.00	0.12	2008.0	0.25

time in all regions but the ANT, which is consistent with the results of the MK trend analysis also showing an increase in severe MHW days in the same regions.

To complement the above investigation, we also performed a change point analysis on the minor and moderate MHWSs, which figure 4 suggest have minimal evolution (or even a modest decline). Indeed, the change point analysis supports this inference with effectively all of the regions showing very small or negative slopes (table 4). Similarly, many of the change point p-values indicate no significant change. We conclude the temporal evolution in MHW extrema is driven entirely by the severe MHWSs.

4. Discussion

We have introduced a new definition for MHW extrema to explicitly allow for and incorporate spatial coherence within these phenomena. We have constructed and characterized 649 475 MWHSs, the collation of individual MHWEs in space and time, from 49 034 524 MHWEs. The volume V_{MHWS} of the MHWSs ranges from the trivial ($\approx$50 km^2 days) to the extreme (over 10^{10} km^2 days) with the majority following a $\Phi(V_{\mathrm{MHWS}}) \propto V_{\mathrm{MHWS}}^{-2}$ power-law distribution. We find that the most severe MHWSs—those with $V_{\mathrm{MHWS}} > 10^8$ km^2 days—represent $> 70\%$ of the ocean undergoing a MHW extremum. These severe MHWS

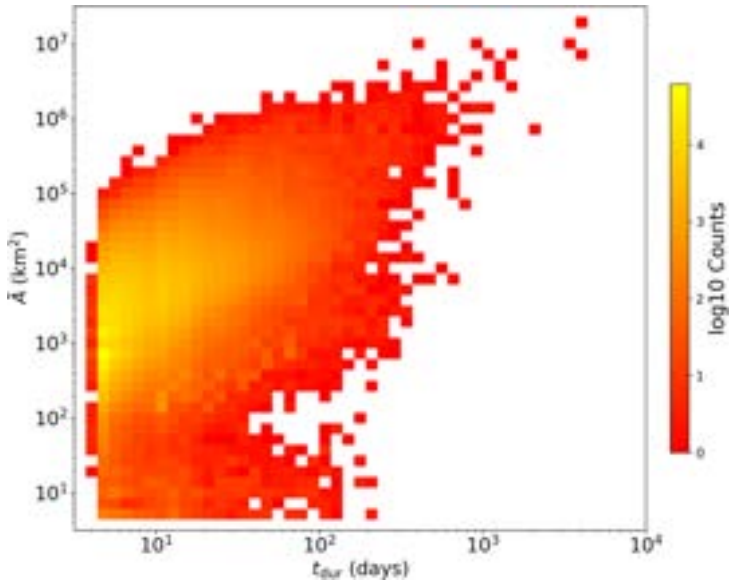

Figure 6. 2D histogram of the characteristic area $\bar{A}$ as a function of duration t_{dur} for the full sample of MHWS. For systems with durations in excess of 10 days, nearly all have large areas ($>10^3$ km^2), indicating significant spatial coherence in MHWs. The highest areas, which correspond to the severe MHWSs, have $\bar{A} > 10^7$ km^2 which is an appreciable fraction of an ocean basin. These results emphasize the importance of spatial extent when characterizing MHWs and estimating their impacts.

have a geographic preference for the central regions of the major basins. More importantly, a trend and change point analysis reveals the severe MHWS have risen rapidly to prominence beginning ≈20 years ago.

A principle implication of the results summarized above is that MHWs exhibit a strong spatial coherence and that this coherence is common and impactful. This may be most evident from the ≈75× agglomeration of MHWEs into MHWSs, i.e. on average 75 MHWEs occupy a common area. The evidence also includes the shallow power-law distribution of maximum area A_{max} indicating a significant integrated contribution from the largest area MHWS. Finally, the majority of the ocean in a MHW state arises in severe MHWS—the largest, coherent phenomena in the ocean. Altogether, we contend the MHWS provide a more natural description of MHW phenomena than the more commonly adopted, spatially independent MHWEs.

We further illustrate this point in figure 6 which shows the measured characteristic areas $\bar{A}$ versus the duration t_{dur} of each MHWS. There is a strong positive correlation between the two quantities, and even shorter duration events have significant areas, e.g. the mean $\bar{A}$ for $t_{dur} = 50$–100 days is 63 500 km^2. At longer durations, one notes that 90% of MHWS with $t_{dur} > 1$ year have $\bar{A} > 10^5$ km^2. The extended sizes of MHWs are fundamental to these extrema, if not their most defining feature.

Another implication of these results is that the spatial coherence of MHWSs yields durations for the extrema that are qualitatively different from those of the standard MHWE definition. This is shown in figure 7 which compares the t_{dur} distributions of MHWSs and MHWEs. Until a duration of $t_{dur} \approx 1$ year, there are 10–100 × more MHWE than MHWS at which point the two distributions cross. Focusing on MHWEs, one may have concluded that MHWs with durations $t_{dur} < 1$ year have the greatest impacts. But when one considers the spatial extent of MHWs, one recovers a set with $t_{dur} \gg 1$ year that drive MHW extrema (e.g. figure 2(d)). These relatively rare, many-year systems have the greatest influence on the ocean surface.

The increase in the fraction of the ocean surface covered by severe MHWS (figure 4) suggests the effective area $\bar{A}$ of the MHWS is also increasing. We examine this inference in figure 8, which plots the annual average of $\bar{A}$ for all MHWS $<\bar{A}>$, with $\bar{A}$ weighted by the number of days Δt the MHWS was active $<\bar{A}>=\sum \bar{A}\,\Delta t/\sum \Delta t$. Indeed, $<\bar{A}>$ has increased nearly 300% from the first decade to the most recent. The figure lends further evidence to a recent and sudden rise in severe MHWS, consistent with the change point analysis of the previous section (figure 5).

The results presented in figure 5, and supported by figures 4 and 8, indicate that nearly the entire ocean has undergone a transition to one where severe MHWS (i.e. large-area, long-duration) are the primary manifestation of today's MHW extrema. Our scientific and community focus, therefore, should be on these few but highly impactful events. Phenomena like the Pacific Warm Blob of 2013–2015 (Bond *et al* 2015, Tseng *et al* 2017) are not one-off, oddball events but the new normal. We argue the principle focus of future MHW analysis should be on the growth, evolution, and implications of these severe MHWS.

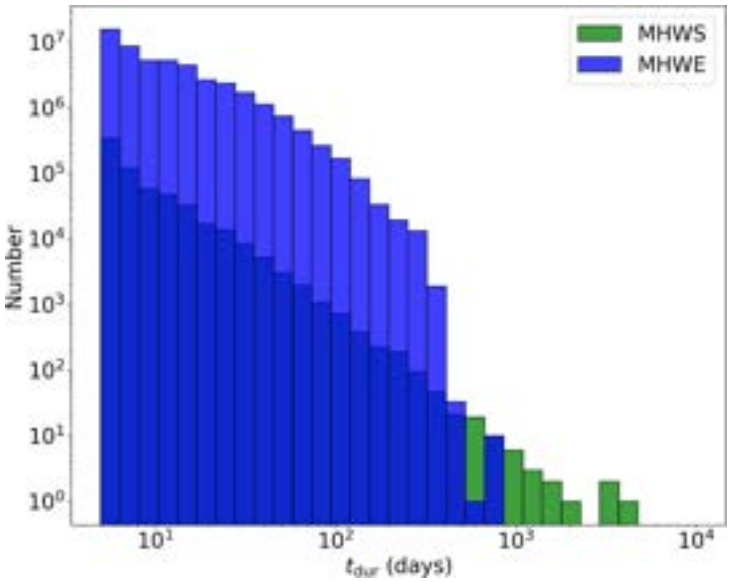

Figure 7. Distributions of the durations t_{dur} of MHWEs and MHWSs. MHWEs are characterized by short to modest durations ($t_{dur} < 1$ year). When one accounts for the spatial coherence of these extrema, the majority of these MHWEs are incorporated into larger duration MHWSs with large areas. The net effect is that MHWs are governed by the rare $t_{dur} \gg 1$ year MHWSs.

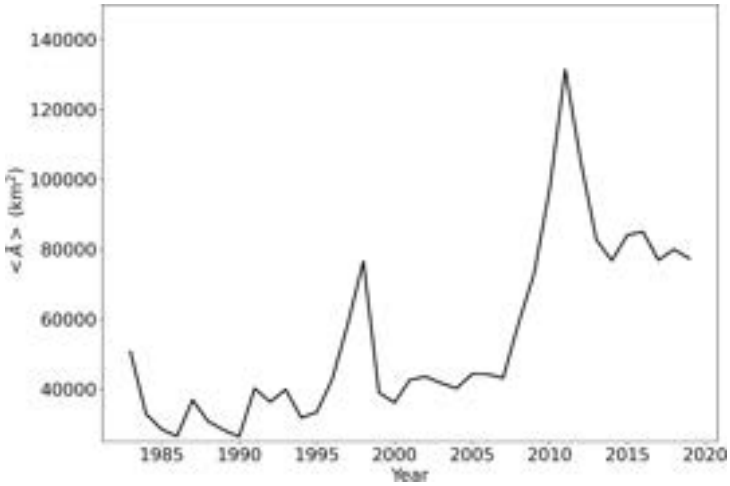

Figure 8. Annual averages for the characteristic area $< \bar{A} >$ of the MHWSs across the full analysis period. Throughout the period, $< \bar{A} >$ exceeds 30 000 km^2, which further emphasizes the strong spatial coherence of MHWs. As important, one observes a sharp rise in $< \bar{A} >$ near year 2007 to values 3 × higher than the first decade. This inflation, which parallels the rise of severe MHWSs (figure 5), signifies a qualitative change in the spatial extent of MHWs.

Other, previous works have also examined the large areas of MHW extrema (Frolicher *et al* 2018, Sen Gupta *et al* 2020). Similar to our MHWS definition, they aggregated neighboring cells on the ocean surface to measure the contiguous areal extent but restricted the aggregation to individual days. Frolicher *et al* (2018) reported a modest increase (∼20%) in the largest area MHWs when dividing their 1982–2016 analysis period in half. This follows the trend displayed in figure 8, although our results indicate a more rapid rise over the past 15 years and a larger (3 ×) increase in the average area. Sen Gupta *et al* (2020), meanwhile, emphasized a higher incidence of large area MHWs during El Niño periods and reported a likely rise in the largest, contiguous MHW on each given day over the past decade.

More recently, Chapman *et al* (2022) applied an archetype analysis of MHW phenomena in the Australasian region to identify large-scale patterns that underly these extrema. They then connect these archetypes to teleconnection patterns of atmospheric and ocean surface modes. Future work might explore the archetypes of the severe MHWSs presented here to identify climate modes driving their formation and evolution. Last, we note the analysis of Sun *et al* (2023) which appeared during the review of this manuscript. Their approach is similar to the MHWS definition introduced here in that it connects MHW extrema in both

space and time, although their analysis focuses primarily on tracking the life-cycle and movement of individual MHW events.

The extended areas of MHWS have consequences for the impacts of these extrema on the ocean. Consider first the potentially harmful effects on ocean biology. To date, MHWs have been implicated for a range of negative impacts (e.g. Smith *et al* 2023) including elevated mortality in fish, mammal, and bird populations (Cavole *et al* 2016, Clement *et al* 2016, Oliver *et al* 2017, Straub *et al* 2022), severe dieback of kelp forests (Pearce and Feng 2013, Smale 2020), coral bleaching and mortality (e.g. Eakin *et al* 2019), and the inspiration of harmful algal blooms (McCabe *et al* 2016, Trainer *et al* 2020). Of these examples cited above, all but one are associated with a severe MHWS. Regarding foundation species (e.g. marine forests, coral reefs), the large and increasing sizes of MHWSs imply ever larger regions affected and, likely, for longer durations. For some areas and populations, one risks complete dieback. Regarding marine megafauna, species that previously could relocate during a MHW (e.g. whales) may no longer have that ability. Last, the larger areas of MHWSs may increase the size and duration of harmful algal blooms with severe, knock-on consequences for coastal life Trainer *et al* (2020). The ominous implication of figure 8 is that ever increasing regions of the ocean are experiencing MHWSs, i.e. no area may be immune to these extrema.

This also has implications for the tracking and prediction of future MHWs (e.g. Jacox *et al* 2022). We surmise that the most effective predictor of where the ocean may next manifest a MHW is the presence of a nearby, severe MHWS. As an example, of the 5.8×10^7 km^2 of the ocean in a MHW state on 1 June 2019, 80% of that area was in existing MHWS on 1 May 2019. And of these, 98% were in severe MHWS. Our results indicate prediction systems should give preference to existing, long-duration MHWS. Despite our own modest success with a model that did not explicitly consider spatial correlation (Giamalaki *et al* 2022), we advocate adopting methods that examine the ocean on much larger scales.

It is worth considering the driving factors for the rapid and continued rise of severe MHWSs. The over-arching factor is the overall warming of the global ocean over the past ∼20 years (Bulgin *et al* 2020), inferred to be the result of anthropogenic influences Oliver *et al* (2019). This has increased the incidence of MHWEs and therefore severe MHWSs in nearly all areas of the ocean (figure 5). To a large extent, this is the combined effects of a warming ocean with a fixed baseline climatology, even one that spans the full analysis period as adopted here. Indeed, adopting a climatology that detrends the mean reduces the incidence of severe MHWSs, but these still dominate the MHW extrema (see supplementary material). The importance of spatial coherence in MHWs is independent of climatology.

5. Summary and concluding remarks

Motivated by theoretical and observational evidence that MHW extrema have large-scale coherence, we implemented a technique from computer vision to construct MHWSs, the aggregation of MHW events in space and time. We then demonstrated that these MHWS follow power-law distributions in duration (t_{dur}^{-3}), maximum area (A_{max}^{-2}), and volume (V_{MHWS}^{-2}). Based on the distribution of V_{MHWS}, we defined three categories of MHWSs: minor, $V_{\text{MHWS}} < 10^5$ vox moderate, $10^5 \leqslant V_{\text{MHWS}} < 10^8$ vox and severe, $V_{\text{MHWS}} \geqslant 10^8$ vox. The latter comprise fewer than 0.05% of the MHWS sample yet deviate from the power-law distribution to dominate the MHW extrema.

Furthermore, we find the trends in MHWs manifests only in these severe MHWSs and with a rapid increase in the interval 2000–2005. This includes all regions of the ocean except the ANT. Given these results, we advocate that future MHW analysis focus primarily on the formation and evolution of severe MHWs, i.e. the forcing mechanisms that generate and sustain large extrema for month/year durations. Of particular interest is whether these are captured in global circulation models intended to track current and future climates.

6. Supplementary materials

6.1. Climatology

The climatology in SST analysis generally refers to the mean SST at a given location on a given DOY. As we are interested in extrema, we measure percentiles of the SST distribution to establish a threshold T_{thresh} which defines an extreme SST excursion. In this analysis, we adopt the 90th percentile T_{90}, i.e. $T_{\text{thresh}} = T_{90}$.

We considered multiple approaches for calculating T_{90} before settling on two for the manuscript: (1) measuring the 90th percentile for the SST distribution at each location over a chosen climatology period;

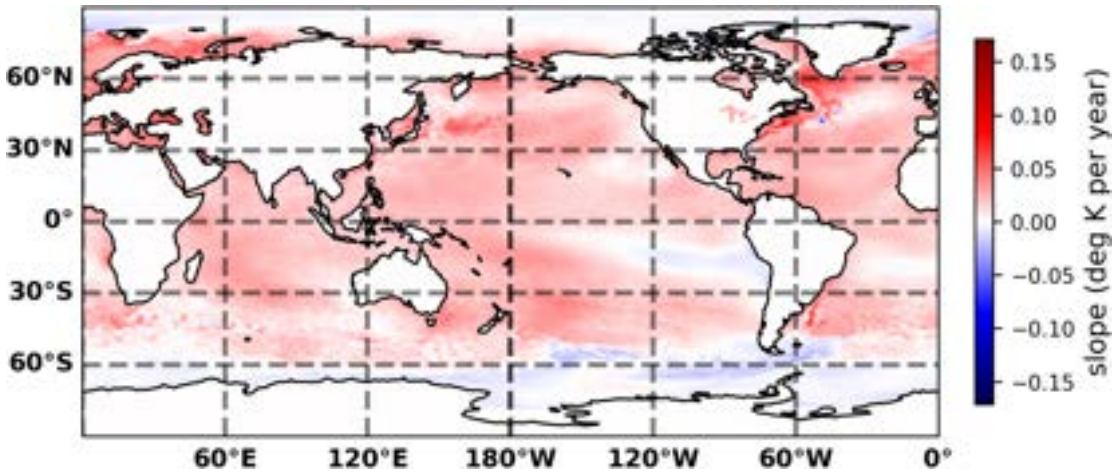

Figure 9. Measured linear trend in SST evolution from 1983–2019, in units of degrees Kelvin per year. The majority of the ocean shows a gradual warming of several hundredths degrees Kelvin per year with notable exceptions of the Arctic and Antarctic oceans and a portion of the southern Pacific. The trend in each cell was removed from the SST values to generate the de-trended climatology considered in this manuscript.

and; (2) calculating T_{90} after modifying the SST values to remove any linear trend (warming or cooling) in the ocean at that location. This 'de-trended' climatology explicitly attempts to correct for long-term ocean warming, i.e. it is designed to examine extrema despite any such trend.

In both cases, our analysis is conducted over the full period (1983–2019, inclusive), where many previous works use only the first 20 years of the period (1983–2012 inclusive). As acknowledged by Hobday *et al* (2016), given the steady increase in average SST over the past ∼15 years using a fixed climatological interval of 1983–2012 lends to a greater incidence of MHWEs in recent years. For example, in 2019 there are portions of the ocean that nearly exceed T_{90} throughout the year.

Within the period one collates the SST measurements from a 11 day interval centered on the DOY. This yields 220 values over the 37 years of the 1983–2019 period modulo missing values in the NOAA OI dataset. The resultant percentile values are then smoothed with a running boxcar average of 31 days centered at the DOY.

Figure 9 shows the linear trend in SST ($d\mathrm{SST}/dt$) at each cell measured over the full period. For the majority of the ocean, there is a modest warming of several hundredths degrees Celsius per year. Notable exceptions are the Arctic and Antarctic oceans and waters at lat $\approx -15°$ in the Pacific Ocean. For the de-trended climatology, we subtract the linear fit from each SST measurement prior to assessing T_{90}. We did the de-trending two ways: (i) locally, i.e. cell by cell and (ii) globally, fitting a trend to the median of all cells but only show results for the former.

Figure 10 compares T_{90} measured from these various approaches to the climatology at an arbitrary location in the Northern Pacific ($lat = 36.125$ deg, $lon = 220.125$ deg). Extending the climatology period to 2019 yields higher T_{90} on each DOY, even for the de-trended climatologies. This leads to fewer extrema at later times in the period. One also notes that extending the climatology to 2019 has a significantly greater impact on T_{thresh} than adjusting for the global warming trend. However, the SST values are also adjusted in the de-trended climatology which reduces MHW phenomena in later years (see below).

Figure 11 shows the distribution of V_{MHWS} vs. t_{dur} for the full sample of MHWSs and the de-trended climatology. As expected, the two metrics are highly correlated. There is, however, a substantial scatter about the main trend, especially for the normal set of MHWSs ($V_{\mathrm{MHWS}} \sim 10^3 - 10^5$ vox, $t_{\mathrm{dur}} \sim 50 - 300$ days). Meanwhile, the severe MHWS all exhibit $t_{\mathrm{dur}} > 100$ days with several exceeding 1000 days. We have marked on this figure several MHWS discussed at length in previous literature (e.g. Hobday *et al* 2018) which are naturally recovered by our algorithm.

To explore the effects of climatology on the primary results of this manuscript, we present figures 12 and 13 which show the distributions of MHWS properties and time evolution for the de-trended climatology. Qualitatively, the results are similar. The t_{dur}, A_{max}, and V_{MHWS} values follow power-law distributions with exponents very similar to those of the fiducial climatology. Furthermore, severe MHWS

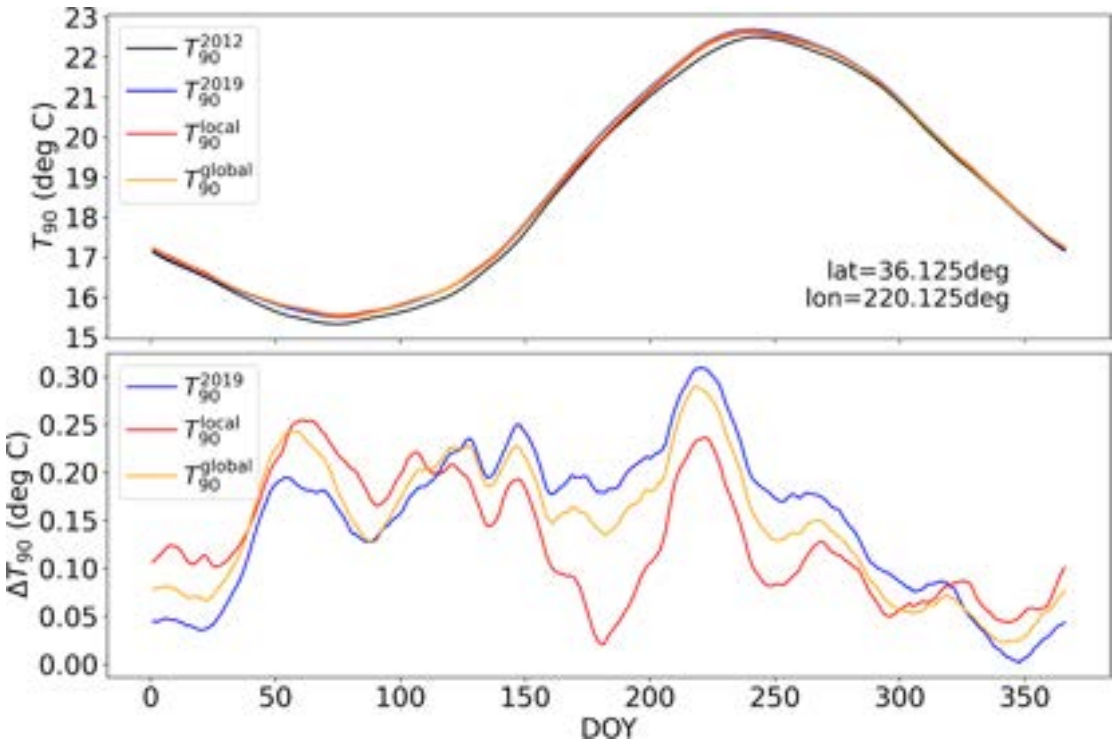

Figure 10. (*upper panel*) Temperature thresholds T_{90} versus day of year *DOY* at an arbitrary location in the northern Pacific. The curves show various treatments for defining T_{90}: (black) T_{90}^{2012}, the 90th percentile of the SST distribution on the given *DOY* based on the 1983–2012 climatology; (blue) T_{90}^{2019}, same as above but including the years through 2019; (red) T_{90}^{local}, same as T_{90}^{2019} but adjusting for trend in warming/cooling of the ocean as described in figure 9 (see text for details). (orange) T_{90}^{global}, also de-trends the SST values but from the global median. All of these other T_{90} definitions exceed the measurements from the 1983–2012 climatology. (*lower panel*) Difference in the threshold temperature ΔT_{90} relative to T_{90}^{2012} for the other three climatologies. Note that the de-trended climatologies tend to show smaller ΔT_{90} values because the range of corrected SST values has been reduced.

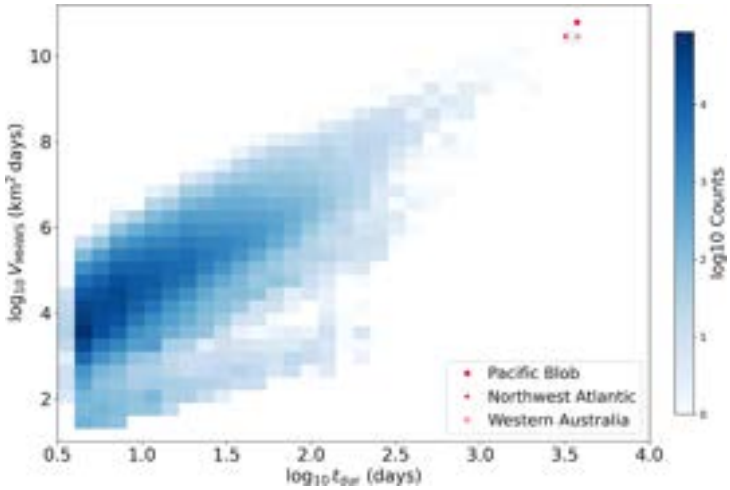

Figure 11. Histogram depicting the relatively tight relation between V_{MHWS} and t_{dur}. The severe MHWS, defined as those with $V_{MHWS} > 10^8$ vox, are almost entirely those with $t_{dur} > 300$ days. Several of the severe MHWSs that contiain prevoiusly studied MHW events are marked with red symbols (see Hobday *et al* 2018).

dominate the total volume of the ocean that enters a MHW state. As expected, the temporal evolution (figure 13) does show a smaller rise in incidence over the past decade but one still identifies the rise in severe MHWSs over the past decade.

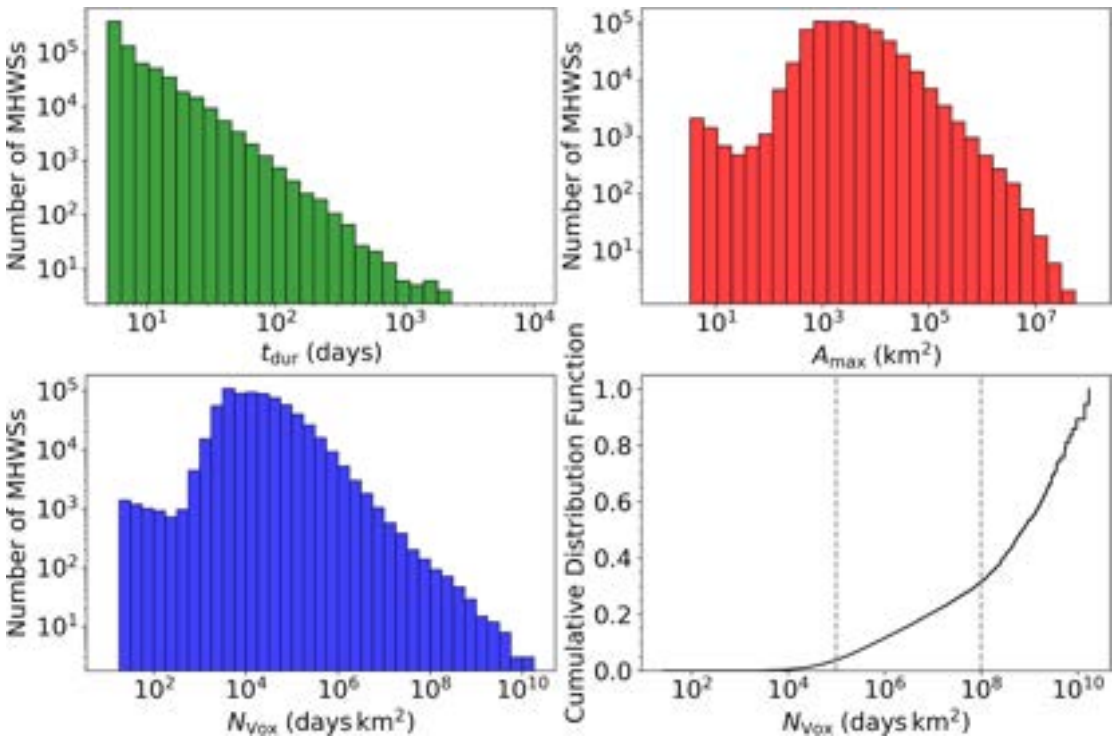

Figure 12. Properties of the MHWS derived with the locally de-trended climatology. Qualitatively, the distributions of duration, maximum area, and volume follow the results for our fiducial climatology (figure 2). Quantitatively, these are fewer severe MHWS, especially those with durations longer than 1 year.

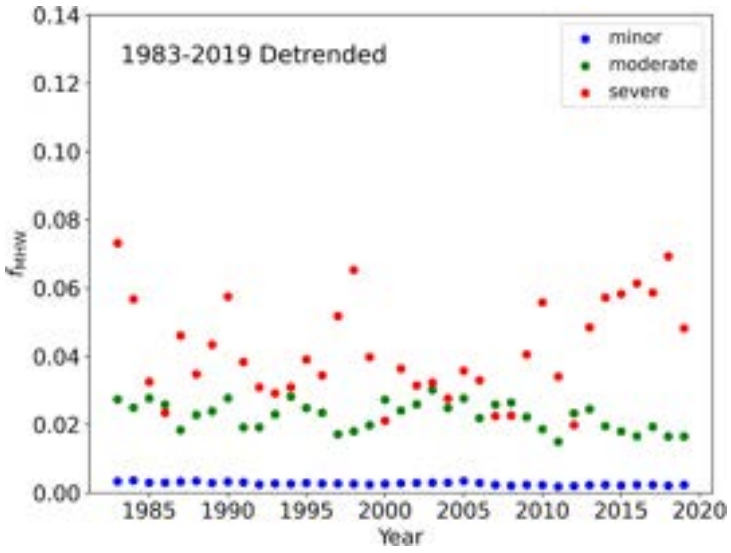

Figure 13. Time series for the fraction of the ocean surface f_{MHW} that in a given year exhibits one of the three MHWS states: minor (blue), moderate (green), severe (red). These results are for the locally de-trended climatology which yields smaller f_{MHW} and weaker trends than the fiducial climatology. Nevertheless, one still identifies a rise in severe MHWSs over the past decade. This feature indicates the recent increase in MHW extrema is non-linear.

Data availability statement

All of the software developed for this manuscript is available in GitHub repositories. For the climatology and MHWE calculations, we started with the Python code developed by E. Oliver (https://github.com/ecjoliver/marineHeatWaves). We modified these to speed-up performance, testing during development that we

reproduced identical results. We then developed alternative climatologies. Our fork of Dr Oliver's repository is here: https://github.com/profxj/marineHeatWaves (Prochaska 2022b). For MHWSs, we developed a separate repository found at https://github.com/profxj/mhw_analysis (Prochaska 2022a). This includes all of the Python scripts required to generate the manuscript figures and tables.

The primary data products of our work are: (1) climatologies, stored as individual netcdf files; (2) databases of MHWEs, stored as SQL data files and *parquet* files; and (3) tables of MHWSs, stored as CSV files. We also generated simple 'movies' of several severe MHWSs as .mov files. All of these are staged on the Dryad long-term archival system at the University of California.

The data that support the findings of this study are openly available at the following URL/DOI: 10.5281/zenodo.7029722.

Acknowledgments

J X P thanks the University of California for supporting his research in Oceanography.

ORCID iD

J Xavier Prochaska https://orcid.org/0000-0002-7738-6875

References

Barbeaux S J, Holsman K and Zador S 2020 Marine heatwave stress test of ecosystem-based fisheries management in t he gulf of alaska pacific cod fishery *Front. Mar. Sci.* **7** 703

Bond N A, Cronin M F, Freeland H and Mantua N 2015 Causes and impacts of the 2014 warm anomaly in the NE pacific *Geophys. Res. Lett.* **42** 3414–20

Bulgin C E, Merchant C J and Ferreira D 2020 Tendencies, variability and persistence of sea surface temperature anomalies *Sci. Rep.* **10** 7986

Cantalupo S, Arrigoni-Battaia F, Prochaska J X, Hennawi J F and Madau P 2014 A cosmic web filament revealed in Lyman-α emission around a luminous high-redshift quasar *Nature* **506** 63–66

Cavole L M *et al* 2016 Biological impacts of the 2013–2015 warm-water anomaly in the northeast pacific: winners, losers and the future *Oceanography* **29** 273–85

Chapman C, Monselesan D, Risbey J, Feng M and Sloyan B 2022 A large-scale view of marine heatwaves revealed by archetype analysis *Nature Commun.* **13** 7843

Clement A *et al* 2016 Exceptional summer conditions and HABs of pseudochattonella in southern chile create record impacts on salmon farms *Harmful Algae News* **53** 1–3

Eakin C M, Sweatman H and Brainard R E 2019 The 2014–2017 global-scale coral bleaching event: insights and impacts *Coral Reefs* **38** 539–45

Frolicher T L, Fischer E M and Gruber N 2018 Marine heatwaves under global warming *Nature* **560** 360–4

Giamalaki K, Beaulieu C and Prochaska J X 2022 Assessing predictability of marine heatwaves with random forests *Geophys. Res. Lett.* **49** e2022GL099069

Hobday A J *et al* 2016 A hierarchical approach to defining marine heatwaves *Prog. Oceanogr.* **141** 227–38

Hobday A J *et al* 2018 Categorizing and naming marine heatwaves *Oceanography* **31** 162–73

Holbrook N *et al* 2019 A global assessment of marine heatwaves and their drivers *Nat. Commun.* **10** 2624

Jacox M G *et al* 2022 Global seasonal forecasts of marine heatwaves *Nature* **604** 486–90

Jacox M, Alexander M, Bograd S and Scott J 2020 Thermal displacement by marine heatwaves *Nature* **584** 82–86

Johnson G C and Lyman J M 2020 Warming trends increasingly dominate global ocean *Nat. Clim. Change* **10** 757–61

Kendall M G 1948 *Rank correlation methods* 4th edn (London: Griffin)

Laufkötter C, Zscheischler J and Frölicher T L 2020 High-impact marine heatwaves attributable to human-induced global warming *Science* **369** 1621–5

Lenanton R, Dowling C, Smith K, Fairclough D and Jackson G 2017 Potential influence of a marine heatwave on range extensions of tropical fishes in the eastern indian ocean—invaluable contributions from amateur observers *Reg. Stud. Mar. Sci.* **13** 19–31

Mann H B 1945 Non-parametric test against trend *Econometrica* **13** 245–95

McCabe R M *et al* 2016 An unprecedented coastwide toxic algal bloom linked to anomalous ocean conditions *Geophys. Res. Lett.* **43** 10366–76

Mills K E *et al* 2013 Fisheries management in a changing climate: lessons from the 2012 ocean heat wave in the northwest atlantic *Oceanography* **26** 191–5

Oliver E C J *et al* 2019 Projected marine heatwaves in the 21st century and the potential for eco logical impact *Front. Mar. Sci.* **6** 1–12

Oliver E C J, Benthuysen J A, Bindoff N L, Hobday A J, Holbrook N J, Mundy C N and Perkins-Kirkpatrick S E 2017 The unprecedented 2015/16 Tasman Sea marine heatwave *Nat. Commun.* **8** 1–12

Oliver E C J, Benthuysen J A, Darmaraki S, Donat M G, Hobday A J, Holbrook N J, Schlegel R W and Sen Gupta A 2021 Marine heatwaves *Annu. Rev. Mar. Sci.* **13** 313–42

Oliver E *et al* 2018 Longer and more frequent marine heatwaves over the past century *Nat. Commun.* **9** 1324

Pearce A F and Feng M 2013 The rise and fall of the "marine heat wave" off western australia during the summer of 2010/2011 *J. Mar. Syst.* **111–112** 139–56

Perkins-Kirkpatrick S 2015 A review on the scientific understanding of heatwaves—their measurement, driving mechanisms and changes at the global scale *Atmos. Res.* **164–165** 242–67

Pettitt A N 1979 A non-parametric approach to the change-point problem *J. R. Stat. Soc.* C **28** 126–35
Piatt J F *et al* 2020 Extreme mortality and reproductive failure of common murres resulting from the northeast pacific marine heatwave of 2014–2016 *PLoS One* **15** 1
Pohlert T 2020 trend: non-parametric trend tests and change-point detection, r package version 1.1.2 (https://doi.org/10.13140/RG.2.1.2633.4243)
Prochaska J X 2022a Marine heat wave system analysis (https://doi.org/10.5281/zenodo.7029722)
Prochaska J X 2022b Marine heat waves (https://doi.org/10.5281/zenodo.7029736)
Reynolds R W, Smith T M, Liu C, Chelton D, Casey K S and Schlax M G 2007 Daily high-resolution-blended analyses for sea surface temperature *J. Clim.* **20** 5473–96
Roemmich D, Church J, Gilson J, Monselesan D, Sutton P and Wijffels S 2015 Unabated planetary warming and its ocean structure since 2006 *Nat. Clim. Change* **5** 240–5
Rogers L A, Wilson M T, Duffy-Anderson J T, Kimmel D G and Lamb J F 2021 Pollock and "the blob": impacts of a marine heatwave on walleye pollock early life stages *Fish. Oceanogr.* **30** 142–58
Sen Gupta A *et al* 2020 Drivers and impacts of the most extreme marine heatwaves events *Sci. Rep.* **10** 19359
Shapiro L and Stockman G 2001 *Computer Vision* (Upper Saddle River, NJ: Prentice-Hall)
Smale D A 2020 Impacts of ocean warming on kelp forest ecosystems *New Phytol.* **225** 1447–54
Smith K E *et al* 2023 Biological impacts of marine heatwaves *Annu. Rev. Mar. Sci.* **15** 119–45
Straub S C, Wernberg T, Marzinelli E M, Vergés A, Kelaher B P and Coleman M A 2022 Persistence of seaweed forests in the anthropocene will depend on warming and marine heatwave profiles *J. Phycol.* **58** 22–35
Sun D, Jing Z, Li F and Wu L 2023 Characterizing global marine heatwaves under a spatio-temporal framework *Prog. Oceanogr.* **211** 102947
Trainer V L, Moore S K, Hallegraeff G, Kudela R M, Clement A, Mardones J I and Cochlan W P 2020 Pelagic harmful algal blooms and climate change: lessons from nature's experiments with extremes *Harmful Algae* **91** 101591
Tseng Y-H, Ding R and meng Huang X 2017 The warm Blob in the northeast Pacific—the bridge leading to the 2015/16 El Niño *Environ. Res. Lett.* **12** 054019
Vogt L, Burger F A, Griffies S M and Frölicher T L 2022 Local drivers of marine heatwaves: a global analysis with an earth system model *Front. clim.* **4** 847995
Zhu Z, Qu P, Fu F, Tennenbaum N, Tatters A O and Hutchins D A 2017 Understanding the blob bloom: warming increases toxicity and abundance of the harmful bloom diatom pseudo-nitzschia in california coastal waters *Harmful Algae* **67** 36–43